Available online at www.sciencedirect.com
ScienceDirect
Journal of Magnetism and Magnetic Materials 317 (2007) 34–40
Journal of magnetism and magnetic materials
www.elsevier.com/locate/jmmm

Motions of magnetic nanosphere under the magnetic field in the rectangular microchannel

Jaemoon Yang[a,1], Joseph Park[a,2], Jaemin Lee[a,3], Bumjun Cha[a,4], Yongjin Song[b,5], Ho-Geun Yoon[c,6], Yong-Min Huh[d,7], Seungjoo Haam[a,*]

[a]*Department of Chemical Engineering, College of Engineering, Yonsei University, Seoul 120-749, South Korea*
[b]*Department of Physics, College of Natural Science, Ajou University, Suwon 433-749, South Korea*
[c]*Department of Biochemistry and Molecular Biology, Center for Chronic Metabolic Disease Research, College of Medicine, Yonsei University, Seoul 120-752, South Korea*
[d]*Department of Radiology, College of Medicine, Yonsei University, Seoul 120-752, South Korea*

Received 3 October 2006; received in revised form 2 April 2007
Available online 19 April 2007

Abstract

The nano-sized magnetite and the magnetic nanospheres (MNS) were synthesized for biomedical applications by co-precipitation method and emulsion solvent evaporation method, respectively. The prepared magnetite and the MNS (~250 nm) exhibited superparamagnetic behaviors with the saturation of magnetization of 52.6 and 38.7 emu/g, respectively. The size, distribution and morphology were investigated by light scattering and electron microscopy. The motions of the MNS under the magnetic field in rectangular microchannel were investigated by using the particle tracking velocimetry (PTV) method. The particle motions due to both the fluid flow and the magnetic field were calculated and the experimentally observed data were in good agreement with theoretical model.

PACS: 74.25.Ha

Keywords: Magnetite; Magnetic nanosphere; Biomedical; PTV

1. Introduction

The magnetic nanoparticles are attractive materials for biomedical application such as hyperthermia, immunoassay, cell separation, magnetic resonance imaging and drug delivery [1–10]. Among them, the magnetite (Fe_3O_4) is a most suitable magnetic material for bioapplications and have characterized in many aspects. The magnetite has demonstrated a low toxicity and well tolerated in the human body [11]. Furthermore, for nano-sized magnetite, biodegradation can occur in the lysosomes of monocyte phagocytes system cells [12]. These magnetic nanoparticles can be coated with surfactants in a liquid carrier and suspended under dispersion medium water or oil. Due to their size and magnetism, magnetic nanoparticles present superparamagnetic behavior that is proper to apply for drug delivery and separation systems because of magnetic reversibility [13]. Magnetic nanoparticles can align and aggregate by the magnetic field and disperse in the medium reversibly after the magnetic field was removed. These magnetic nanoparticles were synthesized by co-precipitation [14–16], thermal decomposition [17,18] and

*Corresponding author. Tel.: +82 2 2123 2751; fax: +82 2 312 6401.
E-mail addresses: 177hum@yonsei.ac.kr (J. Yang), parkys5001@yonsei.ac.kr (J. Park), jpmini@yonsei.ac.kr (J. Lee), laerian@yonsei.ac.kr (B. Cha), yjsong@ajou.ac.kr (Y. Song), yhgeun@yumc.yonsei.ac.kr (H.-G. Yoon), ymhuh@yumc.yonsei.ac.kr (Y.-M. Huh), haam@yonsei.ac.kr (S. Haam).
[1]Tel.: +82 2 2123 3554; fax: +82 2 312 6401.
[2]Tel.: +82 2 2123 3554; fax: +82 2 312 6401.
[3]Tel.: +82 2 2123 3554; fax: +82 2 312 6401.
[4]Tel.: +82 2 2123 3554; fax: +82 2 312 6401.
[5]Tel.: +82 31 219 2301; fax: +82 31 214 1500.
[6]Tel.: +82 2 2228 1683; fax: +82 2 312 5041.
[7]Tel.: +82 2 2228 2375; fax: +82 2 362 8647.

0304-8853/$ - see front matter © 2007 Published by Elsevier B.V.
doi:10.1016/j.jmmm.2007.04.008

microemulsion [19] method. Among them, the co-precipitation method is preferred method for mass production and commercially used in many fields. The motions of these magnetic particles under the magnetic field are very important to comprehend the mechanism of magnetic delivery and separations for biomedical applications. Many researchers have studied the trajectories and the movements of the magnetic particles for many decades [20–22]. In this study, the nano-sized magnetite was synthesized by co-precipitation method and the magnetic nanospheres (MNS) was prepared with the magnetite by emulsion solvent evaporation method. The crystallinity of magnetite was analyzed by X-ray diffraction (XRD) and saturation of magnetization and magnetic susceptibility of magnetic particles were evaluated by vibration sample magnetometer (VSM). The size and morphology of prepared particles were characterized by dynamic laser scattering (DLS) and transmittance electron microscope (TEM), respectively. The motions of MNS under the magnetic field in the rectangular microchannel were estimated using a microscope and image processing system. The captured series images by CCD camera were analyzed using particle tracking velocimetry (PTV) method [23,24]. The experimental data were compared with theoretical results.

2. Materials and methods

2.1. Materials

Ferric chloride anhydrous ($FeCl_3$), ferrous chloride tetrahydrate ($FeCl_2 \cdot 4H_2O$) and polyvinyl alcohol (M.W. 15,000–20,000) was purchased from the Aldrich Chemical Co. (USA). Chloroform and ammonium hydroxide (~30%) were purchased from Duksan Pure Chemicals Co. (Korea). All other chemicals were of analytical grade.

2.2. Synthesis of nano-sized magnetite

The nano-sized magnetite was synthesized by co-precipitation method using an aqueous Fe^{3+}/Fe^{2+} solution and concentrated ammonium hydroxide [14]. A total of 21.0 g of $FeCl_3$ and 17.3 g of $FeCl_2 \cdot 4H_2O$ were dissolved in 50 mL distilled water and 40 mL of ammonium hydroxide were added rapidly. After the co-precipitation of magnetic particles, oleic acid was added and the suspension was heated to 80 °C for 30 min. The products washed using distilled water [15].

2.3. MNS by emulsion solvent evaporation method

Prepared magnetites (20 mg) were dissolved in 10 mL of dichloromethane. The organic phase was added into 20 mL of aqueous phase containing stabilizer (polyvinyl alcohol). After mutual saturation of organic and continuous phase, the mixture was emulsified for 10 min with ultrasonicator (ULH700S, Ulssohitech, Korea) at 200 W. After solvent evaporation, sample was purified using filtration and centrifugation at 10,000 rpm for 30 min.

2.4. Characterization of MNS

The size distributions of the magnetite and MNS were analyzed using light scattering (Zetaplus, Brookhaven 9000 instruments). Transmission electron microscopy (JEOL JEM2000, Nikon, Japan) analysis was performed to observe morphology and size of the nanoparticles. The crystallinity of magnetite was confirmed by XRD. The saturation of magnetization was evaluated using VSM (Lakeshore, model 7300). The magnetic contents of the MNS were determined by thermogravity analyzer (TGA).

2.5. Experimental setup for MNS tracking

Fig. 1(a) shows the MNS tracking system. The MNS was affected by magnetic field (cylindrical Nd–Fe–B magnet) and moved in the rectangular microchannel (sq I.D. 500 μm and 54 mm long, Borosilicate, VitroCom Inc.) (Table 1). Magnetic flux density (B) was changed as variations of distance from a magnet. Magnetic flux density was determined using Gauss meter and Hall-effect probe (Model 5080. F.W.Bell, Orlando, FL). Proper flow rate

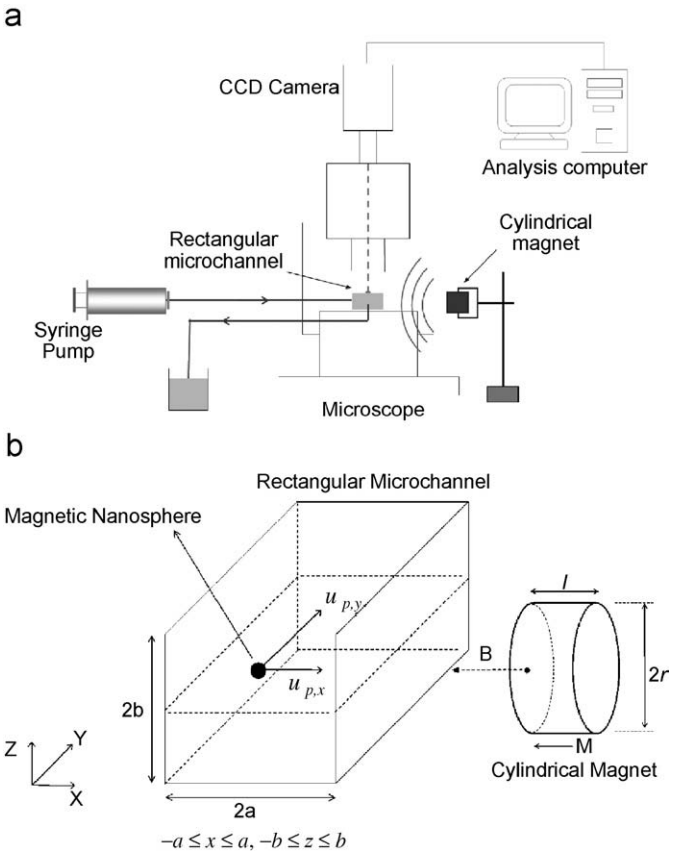

Fig. 1. The MNS tracking system using microscope (a). Cross section of the rectangular microchannel and dimensions of a cylindrical magnet used to calculate flux density at a distance from the magnet surface (b).

Table 1
Dimensions and magnetic properties of various types of cylindrical magnet

Types of magnet	M_1	I_2	M_3	M_4
Diameter ($2r$, mm)	10	10	10	10
Length (l, mm)	10	5	3	1
[a]Surface magnetic flux of the magnet (mt)	470	360	270	140

[a]These value were measures using gauss meter at the surface of magnet.

was controlled by the syringe pump (HAMILTON, KDS-100) with 100 μL syringe (HAMILTON).

Visualization of the motion of MNS was accomplished using a single high-speed camera (PLUMPIX, TM-6410) through the microscope (Olympus, BX51) to get simultaneous views of the specific area with dark field condenser. The maximum camera shutter speed was 120 frames per second. The captured images were stored and subsequently analyzed on a high performance computer by C^{++} code.

2.6. Theories for motions of MNS

The motions of MNS under the magnetic field were determined by the Newton's equation [25], which is given by

$$m_p \frac{du_p}{dt} = F_d + F_g + F_m, \tag{1}$$

where F_d is the drag force, F_g is the gravity and buoyancy forces and F_m is the magnetic force. m_p is the mass of MNS and u_p is the velocity of MNS.

The drag force is then given by

$$F_d = \frac{3\pi\eta d_p}{C_c}(u_f - u_p), \tag{2}$$

where η is the fluid viscosity, d_p is the diameter of MNS, u_f is the fluid velocity and C_c is the Stokes–Cunningham slip correction coefficient [26], which is given by

$$C_c = 1 + \frac{2\lambda}{d_p}(1.252 + 0.399e^{-1.1d_p/2\lambda}), \tag{3}$$

where λ is the mean free path.

The gravity and buoyancy forces is given by

$$F_g = \frac{(\rho_p - \rho_f)\pi d_p^3 g}{6}, \tag{4}$$

where ρ_p and ρ_f are the density of the MNS and fluid, g is the vector of gravity.

The magnetic force is given by

$$F_m = V_p \Delta\chi \nabla\left(\frac{B^2}{2\mu_0}\right), \tag{5}$$

where V_p is the MNS volume, $\Delta\chi$ is the difference of magnetic susceptibility between the particle and the fluid, $B^2/2\mu_0$ is the magnetostatic field energy density and μ_0 is the permeability of free space. The magnetic flux density, B is given by [27]

$$B = \frac{B_r}{2}\left[\frac{d+l}{\sqrt{(d+l)^2 + r^2}} - \frac{d}{\sqrt{d^2 + r^2}}\right], \tag{6}$$

where B_r is the remanence or residual induction of the magnet, r is the radius of the magnet, l is the length of the magnet, and d is the distance between the magnet and the specific point.

When the Stokes number is less than unity, it is permissible according to the discussion in the introduction to neglect the particle inertia in the equation of motion [20,23,28]. In addition, the geometry of the interested region is such that magnetic force is perpendicular to the bulk flow direction (treated only in the x–y plane), F_g was neglected [20]. The motions of the MNS are described by the following set of Eqs. (1), (2), (4) and (5):

$$0 = \frac{1}{\tau_p}(u_f - u_p) + \frac{1}{\rho_p}\Delta\chi\nabla\left(\frac{B^2}{2\mu_0}\right). \tag{7}$$

Herein, τ_p was defined by

$$\frac{1}{\tau_p} = \frac{3\pi\eta d_p}{m_p C_c}. \tag{8}$$

The velocity of the MNS ($u_{p,y}$) against y-direction by fluid flow was calculated in the x–y plane (Fig. 1(b)):

$$u_{p,y} = u_{f,y}. \tag{9}$$

The flow velocity of fluid (u_f) in the rectangular channel is determined at $z = 0$, $a = b$. Q is the flow rate [29]. $u_{f,y}$ is the function of the only position x:

$$u_{f,y}(x) = \frac{12Q}{a^2\pi^3}\frac{\sum_{i=1,3,5,\ldots}^{\infty}(-1)^{(i-1)/2}[1 - (1/(\cosh(i\pi/2)))](\cos(i\pi x/2a)/i^3)}{[1 - (192/\pi^5)\sum_{i=1,3,5,\ldots}^{\infty}(\tanh(i\pi/2)/i^5)]}. \tag{10}$$

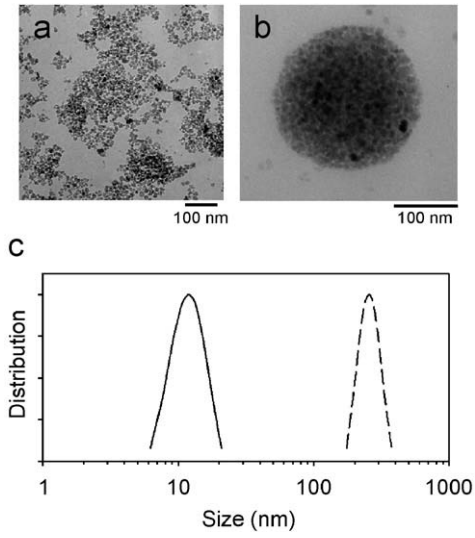

Fig. 2. TEM images of nano-sized magnetite by co-precipitation method (a) and MNS using emulsion solvent evaporation method (b). (c) Size distributions of magnetite and MNS by DLS.

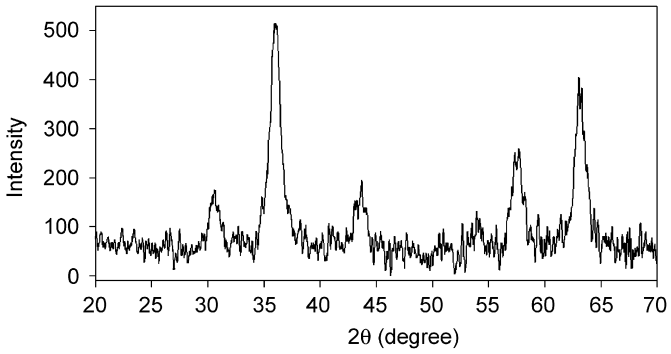

Fig. 3. X-ray diffraction patterns of synthetic magnetite (Fe_3O_4).

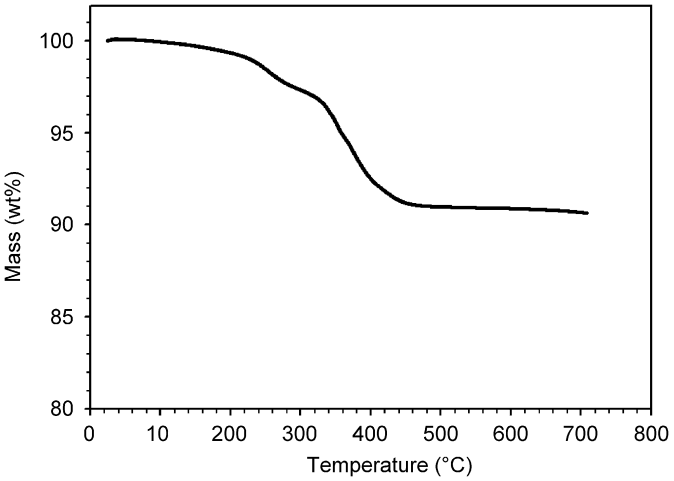

Fig. 4. The magnetite contents of MNS were determined by TGA. Weight loss due to presence of oleic acid and PVA were determined.

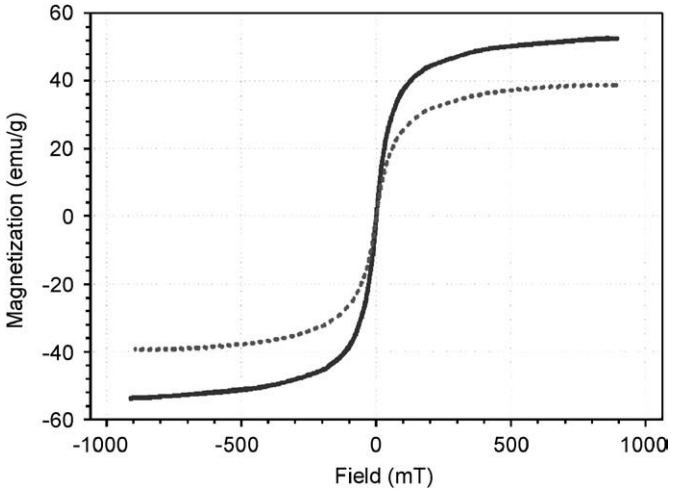

Fig. 5. Magnetization curve for magnetite (—) and magnetic sphere (…) by VSM.

The velocity of the MNS ($u_{p,x}$) against x-direction by magnetic field was then calculated as

$$u_{p,x} = \tau_p \frac{1}{\rho_p} \Delta\chi \nabla \left(\frac{B^2}{2\mu_0} \right). \quad (11)$$

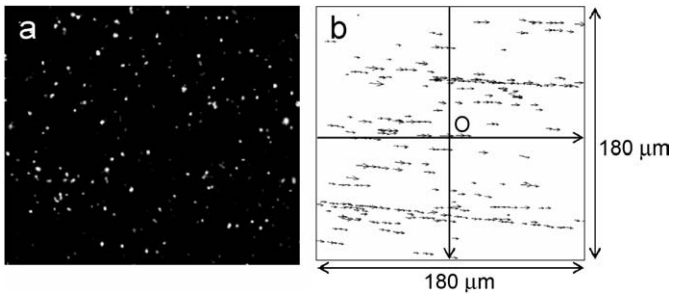

Fig. 6. Dark field microscope image of MNS in the rectangular microchannel (a) and the vector plot of MNS (b) at flow rate of 300 μL/h under the magnetic field (M_1) using microscope (400 ×).

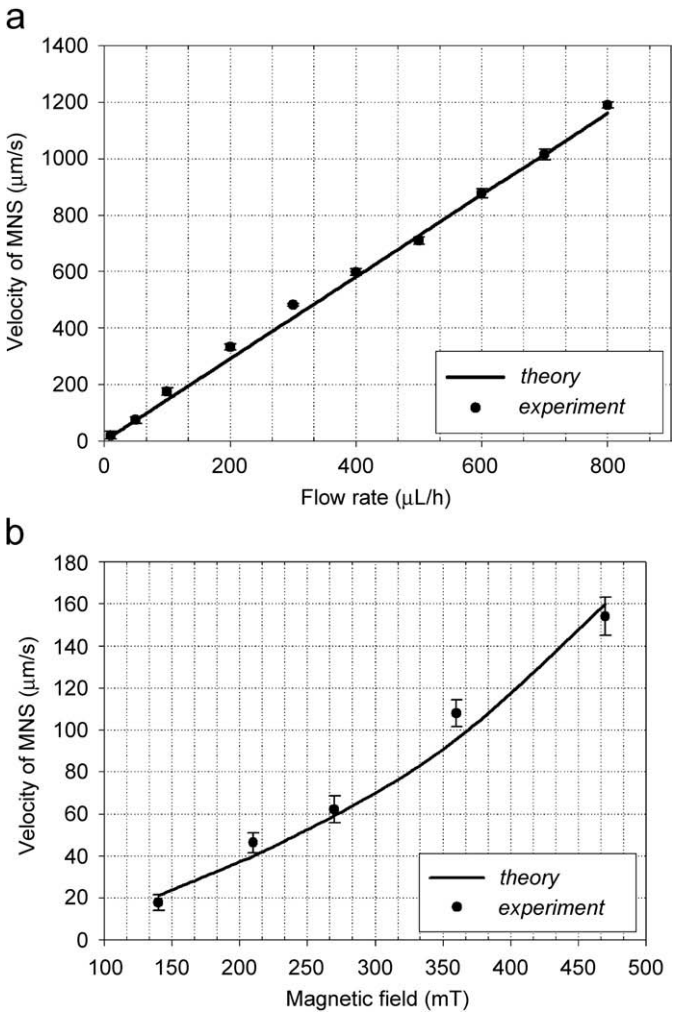

Fig. 7. The theoretical (lines) and experimental (dots) velocities of the MNS without magnetic field (a) and with only magnetic field (no flow) (b) were evaluated.

Finally, the velocity ratio was calculated numerically by analyzing the two component of the velocity of MNS ($u_{p,x}$ and $u_{p,y}$). The motions of MNS were obtained at specific area using

$$\frac{dx}{dy} = \frac{u_{p,x}(x)}{u_{p,y}(x)}. \quad (12)$$

3. Results and discussion

3.1. Properties of magnetite and MNS

The spherical and monodispersed magnetite with a mean diameter of 10 nm was obtained by co-precipitation process (Fig. 2) and XRD patterns of the prepared magnetic nanocrystals were shown in Fig. 3.

The MNS with smooth surfaces and moderately uniform size distributions were obtained by the emulsion solvent evaporation method. The mean size (~250 nm) and the size distribution of MNS were measured by laser scattering (Fig. 2(c)). TEM photography of MNS is shown in Fig. 2(b).

The amount of magnetite in the MNS measured by TGA was determined as 90.5 wt% as shown in Fig. 4 and this value was used for calculating magnetic-induced velocity.

The hysteresis loops of the MNS were observed using a VSM at 300 K (Fig. 5). The prepared MNS exhibited the superparamagnetic behavior without magnetic hysteresis. The saturation of magnetizations (M_s) against magnetite and MNS were 52.6 and 38.7 emu/g at 900 mT, respectively. The M_s of MNS was smaller than that of bulk magnetite because of oxidation during the process, but both particles presented the superparamagnetic behavior.

3.2. Comparisons of the MNS velocities and their ratio

The MNS was visualized using microscope with dark field condenser (Fig. 6(a)). The interested region for visualization was selected with 180 μm × 180 μm at the center of rectangular microchannel. Captured series images were analyzed by PTV algorithm [4,20,22] that was used to calculate the vector plot (Fig. 6(b)) at each condition (specific flow rate and magnetic field). To comprehend the relationship between the flow field and magnetic field, the theoretical and experimental data were compared. In theoretical model, the size of MNS was assumed with 250 nm. Figs. 7(a) and (b) presented the magnitude of

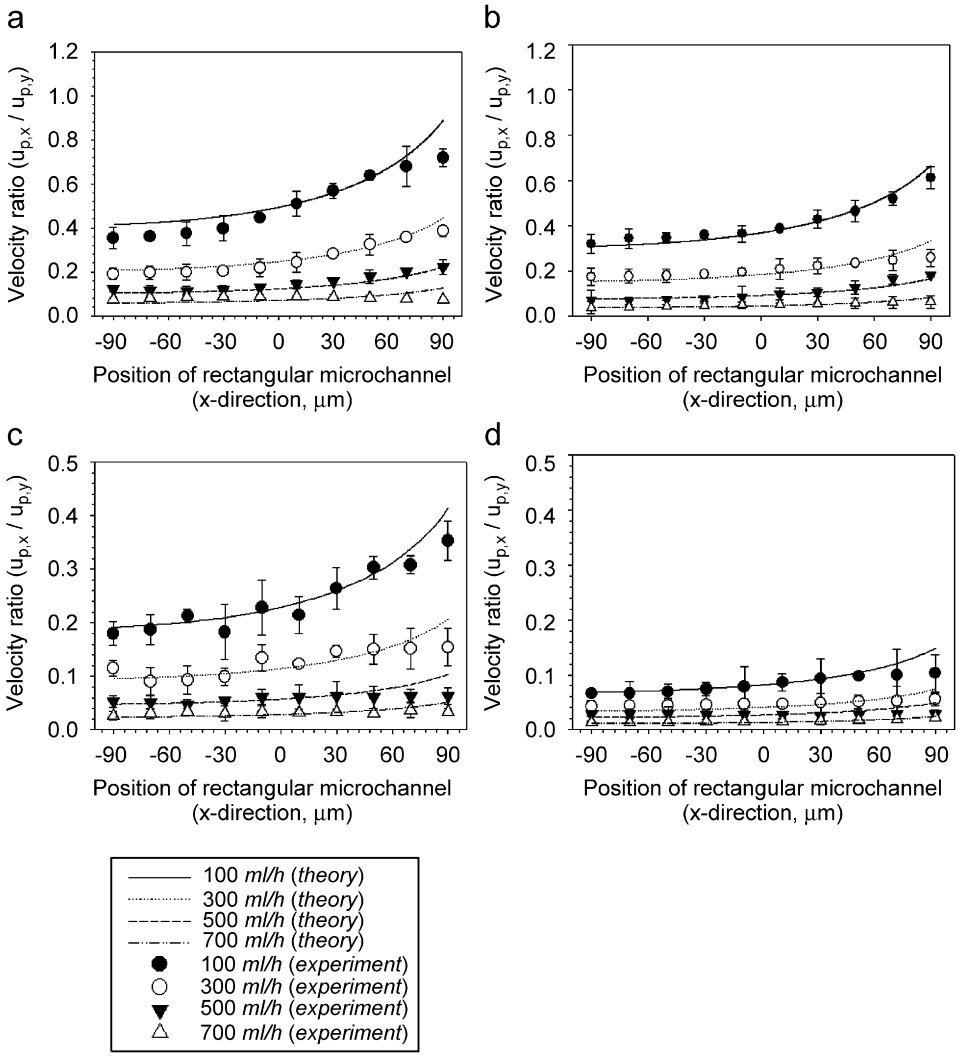

Fig. 8. Theoretical (lines) and experimental (dots) values of the velocity ratio ($u_{p,x}/u_{p,y}$) due to both fluid flow and magnetic field at each position of rectangular channel were obtained using various magnet; (a) M_1, (b) M_2, (c) M_3 and (d) M_4.

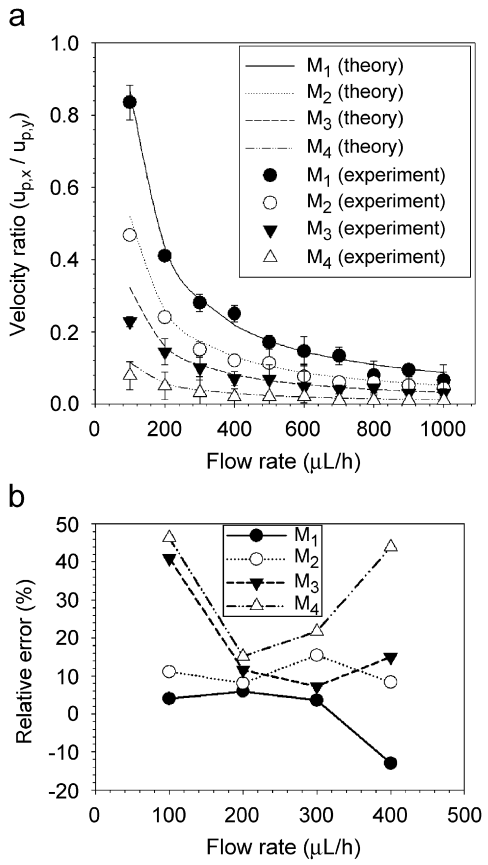

Fig. 9. The velocity ratios of average value at focus region were evaluated under the flow rate and the magnetic field (a) and relative error at slow flow rate (b).

MNS velocities without magnetic field (in the presence of fluid flow) and with only magnetic field (no flow), respectively. The MNS were performed with good flow marker in former case. In latter, however, there was no fluid flow in the microchannel and the MNS were attracted by specific magnetic field toward magnet and deviations of theoretical and experimental results due to thermodynamic hindrance were presented [30].

Fig. 8 shows the velocity ratio of fluid flow-induced velocity ($u_{p,y}$) and magnetic-induced velocity ($u_{p,x}$) at specific position. As the distance from the magnet was increased, the MNS velocity ratio ($u_{p,x}/u_{p,y}$) increased gradually in case of both theoretical and experimental results. When lower magnetic field was applied, the velocity ratio value was decreased. These results came from enhanced magnetic force and relative slow fluid flow near the channel side wall.

The average velocity ratios about whole interested region were presented in Fig. 9(a). The magnetic-induced velocities were diminished with increase of the flow rate that decreases the velocity ratio at each magnetic field condition. In addition, relative errors by Eq. (13) revealed generally higher value at slow flow rate and under low magnetic field (Fig. 9(a)). At these conditions, the prepared MNS was influenced by Brownian force that may cause the deviation of between theoretical model and experimental data [30]:

$$\text{Relative error (\%)} = \frac{\text{theoretical value} - \text{experimental value}}{\text{experimental value}} \times 100. \quad (13)$$

4. Conclusion

The nano-sized magnetite and the MNS were prepared by co-precipitation method and emulsion solvent evaporation method, respectively. The crystallinity and magnetic properties of prepared particles analyzed by XRD confirmed that high quality magnetic materials were synthesized. The spherical and monodisperse MNS were confirmed by DLS and TEM. In summary, the motions of the MNS under the magnetic field in rectangular microchannel were efficiently understood by using PTV method. The velocity vectors and their ratio of each axis due to both the fluid flow and the magnetic field are experimentally observed and these results were in good agreement with the theoretical model. These results may apply to engineering process and biomedical application such as cell separation, immunoassay and magnetic drug delivery.

Acknowledgment

This work was supported by KOSEF through National Core Research Center for Nanomedical Technology (R15-2004-024-00000-0 and R01-2006-000-10023-0), the National R&D Program for Cancer Control, Ministry of Health & Welfare, Republic of Korea (0620190-1).

References

[1] A. Jordan, R. Scholz, P. Wust, H.F. Hling, R. Felix, J. Magn. Magn. Mater. 201 (1999) 413.
[2] A. Jordan, R. Scholz, K. Maier-Hauff, M. Johannsen, P. Wust, J. Nadobny, H. Schirra, H. Schmidt, S. Deger, S. Loening, W. Lanksch, R. Felix, J. Magn. Magn. Mater. 225 (2001) 118.
[3] U. Hafeli, W. Schutt, J. Teller, M. Zborowski, Scientific and Clinical Applications of Magnetic Carriers, Plenum press, New York, 1996, 303pp.
[4] M. Zborowski, L. Sun, L.R. Moore, P.S. Williams, J.J. Chalmers, J. Magn. Magn. Mater. 194 (1999) 224.
[5] T. Schneider, L.R. Moore, Y. Jing, S. Haam, P.S. Williams, A.J. Fleischman, S. Roy, J.J. Chalmers, M. Zborowski, J. Biochem. Biophys. Methods 68 (2006) 1.
[6] K.E. McCloskey, J.J. Chalmers, M. Zborowski, Anal. Chem. 75 (2003) 6868.
[7] L.X. Tiefenauer, A. Tschirky, G. Kuhne, R.Y. Andres, Magn. Reson. Imaging 14 (4) (1996) 391.
[8] R. Kopelmana, Y.L. Koo, M. Philbert, B.A. Moffat, G.R. Reddy, P. McConville, D.E. Hall, T.L. Chenevert, M.S. Bhojani, S.M. Buck, A. Rehemtulla, B.D. Ross, J. Magn. Magn. Mater. 293 (2005) 404.
[9] J. Yang, S.-B. Park, H.-G. Yoon, Y.-M. Huh, S. Haam, Int. J. Pharma. 324 (2006) 185.
[10] V. Cabuil, Encyclopedia of Surface and Colloid Science, Marcel Dekker Inc., New York, 2002, 4306pp.

[11] A. Iannone, R.L. Magin, T. Walczack, M. Federico, H.M. Swartz, A. Tomasi, V. Vannini, Magn. Reson. Med. 22 (1991) 435.
[12] E. Okon, D. Pouliquen, P. Okon, Z.V. Kovaleva, T.P. Stepanova, S.G. Lavit, B.N. Kudryavtsev, P. Jallet, Lab. Invest. 91 (1994) 895.
[13] Q.A. Pankhurst, J. Connolly, S.K. Jones, J. Dobson, J. Phys. D 36 (2003) R167.
[14] G.W. Reimers, S.E., Khalafalla, 1974, US Patent No. 3,843,540.
[15] L.P. Ramirez, K. Landfester, Macromol. Chem. Phys. 204 (2003) 22.
[16] R. Massart, E. Dubois, V. Cabuil, E. Hasmonay, J. Magn. Magn. Mater. 149 (1995) 1.
[17] S. Sun, H. Zeng, D.B. Robinson, S. Raoux, P.M. Rice, S.X. Wang, G. Li, J. Am. Chem. Soc. 126 (2004) 273.
[18] W.W. Yu, J.C. Falkner, C.T. Yavuz, V.L. Colvin, Chem. Commun. (2004) 2306.
[19] K.M. Lee, C.M. Sorensen, K.J. Klabunde, G.C. Hadjipanayis, IEEE Trans. Magn. 28 (5) (1992) 3180.
[20] L.R. Moore, M. Zborowski, L. Sun, J.J. Chalmers, J. Biochem. Biophys. Methods 37 (1998) 11.
[21] G. Ahmadi, Q. Chen, J. Aerosol Sci. 29 (9) (1998) 1097.
[22] W.F. Lawson, W.H. Simons, R.P. Treat, J. Appl. Phys. 48 (8) (1977) 3213.
[23] L.R. Moore, M. Zborowski, M. Nakamura, K. McCloskey, S. Gura, M. Zuberi, S. Margel, J.J. Chalmers, J. Biochem. Biophys. Methods 44 (2000) 115.
[24] J.J. Chalmers, S. Haam, Y. Zhao, K. McCloskey, L. Moore, M. Zborowski, P.S. Williams, Biotechnol. Bioeng. 64 (5) (1999) 509.
[25] M. Zborowski, L.R. Moore, P.S. Williams, J.J. Chalmers, Sep. Sci. Technol. 37 (16) (2002) 3611.
[26] A. Li, G. Ahmadi, Aerosol Sci. Technol. 16 (1992) 209.
[27] G.P. Hatch, R.E. Stelter, J. Magn. Magn. Mater. 225 (2001) 262.
[28] W.H. Simons, R.P. Treat, J. Appl. Phys. 51 (1) (1980) 578.
[29] F.M. White, Viscous Fluid Flow, McGraw-Hill, Inc., New York, 1991, pp. 119–122.
[30] D. Gupta, M.H. Peters, J. Colloid Interface Sci. 104 (2) (1985) 375.